ChemComm

COMMUNICATION

View Article Online
View Journal | View Issue

Cite this: *Chem. Commun.*, 2022, **58**, 10357

Received 27th June 2022,
Accepted 18th August 2022

DOI: 10.1039/d2cc03571e

rsc.li/chemcomm

The bimetallic effect promotes the activity of Rh in catalyzed selective hydrogenation of phenol†

Shiwei Li,[ab] Huachao Zhao,[ab] Wei Ran,[a] Jingfu Liu [abc] and Rui Liu *[abc]

Au@RhPd ultrathin nanowires are designed as a highly reactive and selective catalyst for the hydrogenation of phenol under ambient conditions. Au NWs modulate the electronic state of Rh atoms to enhance the adsorption of phenol and desorption of cyclohexanone. Pd works as a cocatalyst to activate H_2 to H* and spillover to Rh sites. This new catalyst shows a turnover frequency of up to 560 h^{-1} for a wide spectrum of phenols with >80% selectivity toward cyclohexanones.

Catalyzed selective hydrogenation is an indispensable toolkit for the chemical industry and produces fine chemicals worth billions of dollars yearly.[1] During this process, the activity of the reactive centers, in most cases, atomic sites of platinum group metals, and the selectivity of the desired products are the most important criteria that determine the overall catalysis performance. The activity is influenced by their capacity to activate chemical bonds with high stability, while the selectivity is determined by the adsorption/desorption balance between key intermediates on the reactive sites. Additionally, the availability of reactive H*, which directly participates in the hydrogenation reaction, is also a crucial factor. Rhodium (Rh) is one of the most active metals in the breaking of stable chemical bonds and is even capable of catalyzing the breaking of the C–F bond with a bond energy of 485 kJ mol^{-1}, as well as hydrogenating aromatic rings at room temperature.[2] However, the intrinsic hydrogenation activity/selectivity of Rh is far from satisfactory. Taking the selective hydrogenation of phenol to cyclohexanone as an example, due to the so-called see-saw relationship between the activity and selectivity,[3] it is very challenging to simultaneously achieve high activity (turnover frequency, TOF > 1 min^{-1} Rh $atom^{-1}$) and high selectivity (>80%) under ambient conditions. Alternative metals like Pd and Ni, are active in the activation of H_2 but have low activity for phenol hydrogenation.[4,5] Harsh reaction conditions, such as high temperatures and high pressures are required to facilitate the overcoming of the high energy barrier referred to in the hydrogenation of the phenol ring. Attempts have been made towards bimetallic catalysts like PtIr,[6] but the activity was also very low. It is highly desirable to uncover the bottleneck step in selective phenol hydrogenation and develop Rh catalysts with high activity/cost ratio to satisfy the ever increasing industrial demand for cyclohexanone.

Herein, we synthesized Rh monolayer (ML) catalysts on ultrathin Au or Au@Ag nanowire (NW) surfaces and studied their catalytic performance in the room-temperature hydrogenation of phenols. As verified by electrochemical experiments and X-ray photoelectron spectroscopy (XPS), the underlying Au core markedly perturbs the electronic state of Rh atoms. Au@Rh has at least 5-fold increase in activity compared with its counterparts. With the further introduction of Pd atoms into the Rh layer, the activity of Rh could be increased by another 50%. Besides, the RhPd ML catalyst also showed satisfactory selectivity of >80% over cyclohexanones. Both theoretical calculations and *in situ* surface-enhanced Raman scattering (SERS) suggest that the superior catalytic activity and selectivity originate from the electronic regulation of Au and the enhanced interaction between Rh and phenol.

Au@Rh NWs were synthesized by our previously reported method.[7] Fig. 1A displays the STEM image of the as-synthesized Au@Rh NWs, while the TEM image, along with those of the counterpart Rh NPs and the commercial Rh/Al_2O_3 catalyst, is shown in Fig. S1 and S2 (ESI†). The absence of Rh nanoparticles suggests the highly efficient deposition of Rh atoms onto Au NWs. We performed atomic resolution spherical aberration corrected high-angle annular dark-field STEM (cs-HAADF-STEM) observation to directly observe the arrangement of Rh atoms on the Au NW surface. An atomic layer with a much

[a] *State Key Laboratory of Environmental Chemistry and Ecotoxicology, Research Center for Eco-Environmental Sciences, Chinese Academy of Sciences, Beijing, 100085, China. E-mail: ruiliu@rcees.ac.cn*
[b] *College of Resources and Environment, University of Chinese Academy of Sciences, Beijing, 100049, China*
[c] *School of Environment, Hangzhou Institute of Advanced Study, UCAS, Hangzhou, 310024, China*

† Electronic supplementary information (ESI) available: Experimental details and supporting figures. See DOI: https://doi.org/10.1039/d2cc03571e

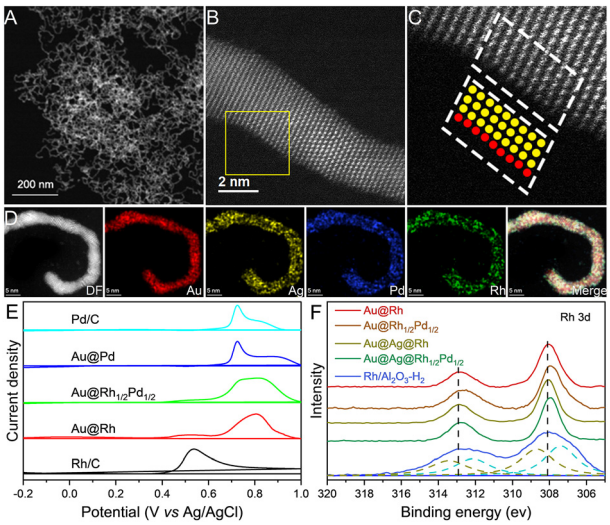

Fig. 1 (A and B) STEM and atomic resolution cs-HAADF-STEM of Au@Rh. (C) The enlarged cs-HAADF-STEM image of the marked area in (B) and the structural model for the four outermost atomic layers. (D) The HAADF-STEM image and the corresponding EDS mappings of $Au@Ag@Rh_{1/2}Pd_{1/2}$. (E) CO stripping voltammetry and (F) the Rh 3d core level-XPS spectra of different NWs.

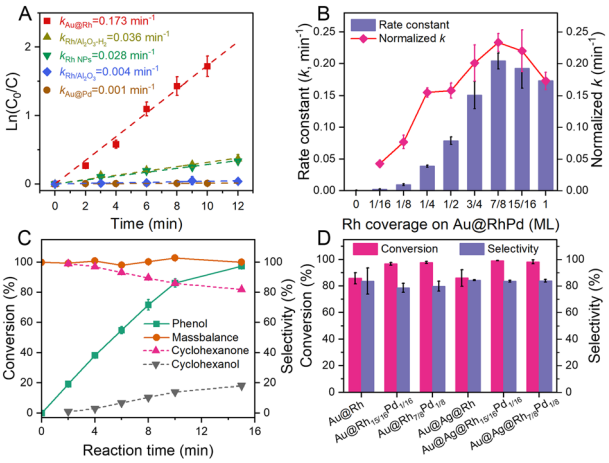

Fig. 2 (A) The first-order kinetics curves and (B) calculated rate constants for different catalysts. (C) Time-dependent catalysis by Au@Rh. (D) Catalytic performance of partial catalysts in the hydrogenation of phenol.

lower image contrast with the Au core and different atomic arrangements was subjected to the epitaxially grown Rh overlayer (Fig. 1B and C). The energy dispersive spectroscopy (EDS) mapping of single NWs reveals that bimetallic metals would also be reduced and deposited on both Au and Au@Ag NWs in the form of mixed monolayers (Fig. 1D and Fig. S3, ESI†) (see infra and additional discussions in the ESI†).

To probe the perturbed electronic state of the Rh ML due to the changed coordination atom/number, we performed CO stripping and XPS analysis.[8] Au@Rh (0.81 V) showed a much higher CO-oxidation potential than Rh/C (0.54 V) (Fig. 1E and Fig. S5, ESI†). This enhanced adsorption of CO on Rh ML implies its lowered d-electron density over that of Rh NPs. This observation indicates that in contrast to Pd gaining d-electrons from Au in Au@Pd,[7] the Au core withdraws electrons from the surface Rh atoms. The changed electronic states of Pd and Rh are directly reflected in their core level-XPS spectra (Fig. 1F and Fig. S7, ESI†). For the Rh/Al_2O_3 reference sample that was pretreated at 200 °C with H_2 (see infra), the Rh 3d spectrum could be deconvoluted into two pairs of peaks, with binding energies (BEs) located at 313.4/308.7 and 312.2/307.4 eV and assigned to Rh^{3+} and Rh^0, respectively. For Au@Rh NWs, the BE of Rh 3d XPS is in the middle of those of Rh^{3+} and Rh^0, directly associated with the electron-deficient nature of the Rh overlayer. Further incorporation of Pd caused considerable shifts of the Rh $3d_{5/2}$ core level peak to lower binding energies, suggesting a charge-transfer to Rh. Accordingly, considerable shifts of Pd $3d_{3/2}$ to higher binding energies were observed for Au@RhPd compared with Au@Pd. These results suggest that the further incorporation of Pd into the Rh ML partially compensated its lowered electron density, implying that it could be finely regulated through the formation of a core–shell nanostructure (Au@Rh) or nanoalloy (RhPd).

The catalytic performance of different Rh catalysts in the hydrogenation of phenol was evaluated. Based on the change in phenol concentration, the reaction kinetics of all the tested catalysts were fit with the first-order kinetic model (Fig. 2A). Control catalysts such as Au, or Au@Pd (k, 0.001 min^{-1}) were almost inactive, in line with their limited activity in phenol hydrogenation under mild conditions. Monometallic Rh catalysts, such as Rh NPs and the commercial Rh/Al_2O_3, showed moderate activity with rate constants of 0.028 and 0.004 min^{-1}. After pretreatment with H_2 at 200 °C for 2 hours, the activity of Rh/Al_2O_3–H_2 increased to 0.036 min^{-1}, thus indicating the key role of the Rh state value in determining the catalytic performance.[3] In contrast, upon deposition onto Au NWs and the formation of Au@Rh, the activity of Rh atoms was largely increased. With quantitative conversion of phenol in 15 min using 1 atom% Rh atoms, Au@Rh showed a high-rate constant of 0.173 min^{-1}, which has an approximately 5-fold increase over that of counterpart monometallic Rh catalysts. The above results unambiguously reveal the fact that the formation of Au@Rh core–shell catalysts is a feasible strategy for promoting the activity of Rh in the catalyzed hydrogenation of phenol.

As a further attempt to increase the activity of Rh in the hydrogenation of phenol, Pd atoms that show high activity in the activation of H_2 into reactive H*, which may spill over to nearby Rh sites,[9] were co-deposited with Rh atoms as a RhPd bimetallic ML. Although Pd was almost totally inactive, the resulting Au@RhPd did show a moderate increase in activity compared with that of Au@Rh (Fig. 2B and Fig. S8, ESI†). Intriguingly, the activity of Au@RhPd shows volcanic dependency on the Rh/Pd ratio and $Au@Rh_{7/8}Pd_{1/8}$ (1/8 refers to the coverage of Pd being 1/8 ML) reached the highest rate constant of 0.204 min^{-1}, an 18% increase over that of Au@Rh (0.173 min^{-1}). If the mass of Rh was taken into consideration, the Rh-mass-normalized rate constants of $Au@Rh_{15/16}Pd_{1/16}$ (0.220 min^{-1}) and $Au@Rh_{7/8}Pd_{1/8}$ (0.233 min^{-1}) were 27%

and 35% higher than that of Au@Rh (0.173 min^{-1}), respectively. Therefore, along with the formation of the Au@Rh core–shell catalyst, the introduction of Pd would further promote the activity of Rh. We further synthesized Au@Ag@RhPd catalysts and evaluated their catalytic hydrogenation of phenol (Fig. S9, ESI†). Like Au@RhPd, Au@Ag@RhPd NWs also showed high activity (0.183 min^{-1}) and coincidentally, Au@Rh and Au@Ag@Rh showed almost identical activity, indicating that Au and Au@Ag cores may play similar roles in promoting the activity of Rh. Furthermore, the highest rate constant was also observed at Au@Ag@$Rh_{7/8}Pd_{1/8}$, which is 0.225 min^{-1} and 10% higher than that of Au@$Rh_{7/8}Pd_{1/8}$. The Rh-mass-normalized activity reached 0.25 min^{-1}, which is 40% higher than that of Au@Rh or Au@Ag@Rh. All the results indicate that Pd enhanced the Rh-catalyzed hydrogenation of phenol.

In addition to activity, the Rh ML catalyst also showed superior selectivity toward cyclohexanone over that of monometallic Rh (Fig. 2C and Fig. S10, ESI†). The selectivity over cyclohexanone was 93% and 82% at 6 and 10 min, respectively and then remained unchanged for Au@Rh. This indicates that a portion of cyclohexanone was over-hydrogenated into cyclohexanol but with low activity. To determine whether the high selectivity over cyclohexanone is a thermodynamically or kinetically favorable result, we hydrogenated cyclohexanone with the designed catalyst (Fig. S11, ESI†). Approximately 10% of cyclohexanone could be rapidly reduced to cyclohexanol in the first 3 min. However, in the subsequent 3 min, only 5% of cyclohexanone was reduced and no further reduction was observed even with the elongation of the reaction time to 1 h, suggesting that the formation of cyclohexanone is more favorable than that of cyclohexanol. The high selectivity of above 80% was observed for all Rh and RhPd ML catalysts (Fig. 2D). Moreover, if a base, c.a., NaOH, was added into the reaction medium, the selectivity over cyclohexanone would further increase to >95%, but at the expense of approximately 30% of activity (Fig. S12, ESI†).

To understand the microscopic mechanism of the AuRh bimetallic effect, we performed systematic kinetics, a thermodynamic analysis and *in situ* SERS study (Fig. 3). First, we explored the kinetic isotope effect (KIE) with the use of D_2 in phenol hydrogenation. A KIE factor (K_{Rh-H}/K_{Rh-D}) of 5.09 was observed in Au@Rh (Fig. 3A and Fig. S13, ESI†), and this value further increased to 5.81 for Au@$Rh_{7/8}Pd_{1/8}$. This large KIE factor indicates that the cleavage of Rh–D is the rate-determining step[10] and reveals that the underlying Au atoms do not change the overadsorption of reactive H* on Rh sites. We then calculated the adsorption energy of phenol onto Rh sites, as its strong adsorption would be favorable for the completion of the binding site with reactive H*. Indeed, upon being deposited onto the Au surface as an overlayer, the adsorption of phenol is enhanced by a large margin (Fig. 3B). This trend is especially evident for both the perpendicular and parallel adsorption configurations, which is exothermic and more facile for the hydrogenation of the benzene ring. Therefore, both the KIE experiment and adsorption calculation reveal that Au accelerates the Rh-catalyzed phenol hydrogenation

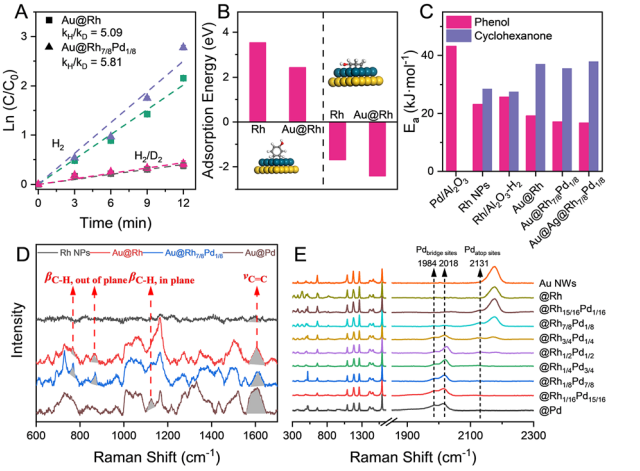

Fig. 3 (A) Primary isotope effect observed for Au@Rh and Au@$Rh_{7/8}Pd_{1/8}$ in phenol hydrogenation. (B) The calculated adsorption energies of phenol with two configurations on Rh and Au@Rh surface. (C) Arrhenius activation energies (E_a) of phenol and cyclohexanone hydrogenation on different catalysts. (D and E) The SERS spectra of phenol and 2,6-DMPI chemisorbed onto different catalysts.

reaction *via* the electronic effect, which enhances the adsorption of phenol and increases its probability of reacting with reactive H*. The further increase in the KIE value induced by the addition of Pd can be attributed to the facile activation of H_2. For the zero-point energy difference between isotopic isomers, the activation of H_2 on Pd is more facile than D_2, resulting in a KIE(K_{Pd-H}/K_{Pd-D}) larger than 1. Since Pd sites themselves are ineffective active centers for the activation of phenol, the reactive H* would spillover to nearby Rh atoms for the hydrogenation reaction. This was reflected in the larger KIE in Au@RhPd than Au@Rh. (Fig. 3A)

We further analyzed the activation energies for the hydrogenation of phenol and cyclohexanone (E_a, Fig. 3C). A high E_a of 43.08 kJ mol^{-1} was observed for the Pd catalyst, attributed to the low intrinsic activity of the Pd monometallic catalyst. All Rh catalysts, including commercial Rh/Al_2O_3, Rh NPs and Au@Rh NWs, showed low E_a of 25.65, 23.14 and 19.14 kJ mol^{-1}, respectively. The relatively low E_a is in line with the fact that Rh could catalyze the hydrogenation of phenol at room temperature. Moreover, the even lower E_a for Au@Rh is over that of the monometallic Rh catalyst, indicating that the Au core could significantly reduce the energy barrier for the Rh-activated aromatic ring. The activation energies of Au@$Rh_{7/8}Pd_{1/8}$ and Au@Ag@$Rh_{7/8}Pd_{1/8}$ further decreased to 17.07 and 16.69 kJ mol^{-1}, respectively, indicating that Pd can notably enhance the ability of Rh to activate the aromatic ring. On the other hand, both Rh ML and RhPd ML showed a relatively large E_a for the hydrogenation of cyclohexanone, which increased from 28.5 for the Rh monometallic catalyst to 35–37 kJ mol^{-1}. Therefore, the presence of the Au core and Pd neighboring atoms not only lowered the energy barrier for the hydrogenation of phenol but also suppressed its further hydrogenation into cyclohexanol and guaranteed the effective generation of cyclohexanone as the favored product.

Based on the relative intensity of the Raman band associated with the out-of-plane/in-plane vibration of C–H,[7,11] the adsorption configuration of phenol molecules onto different reactive sites could be deduced (Fig. 3D). For Au@Pd, the peak at 1126 cm^{-1} assigned to the in-plane vibration of β_{C-H}, indicates the perpendicular adsorption of phenol, an unfavorable configuration for its subsequent activation and hydrogenation. For Au@Rh and Au@RhPd, the strong out-of-plane vibration related Raman bands imply parallel adsorption, and the strong π–π interaction between the aromatic ring and active sites.[12] Therefore, *in situ* SERS reveals the different adsorption configurations of phenol onto Rh and Pd sites and the presence of trace amounts of Pd has a negligible influence on this. Based on the clarified adsorption behaviors, we further calculated the adsorption energy of phenol and cyclohexanone onto different reactive sites (Fig. S14, ESI†). Again, all Rh or RhPd ML sites showed higher adsorption energy for phenol but much lower adsorption energy for cyclohexanone. The enhanced adsorption of phenol is favorable for its complete binding sites with reactive H*, while the lowered affinity for cyclohexanone is meaningful for the fast regeneration of the reactive center and suppression of its overhydrogenation.

We also employed SERS to determine the best catalysis performance of $Rh_{7/8}Pd_{1/8}$. For both $Au@Rh_{7/8}Pd_{1/8}$ and $Au@Ag@Rh_{7/8}Pd_{1/8}$, the relative intensity of the Raman band for Pd atop sites in the SERS spectra of chemisorbed 2,6-DMPI reached the highest (Fig. 3E and Fig. S16, ESI†). This result reflects that the relative abundance of isolated Pd sites reached a maximum. The most plausible explanation for this is, under this circumstance, that the abundant isolated Pd sites are sufficient for the generation of H*, while Rh sites with appropriate coordination numbers are also retained for the activation/hydrogenation of the phenol ring. As discussed in previous works that the surface structure influences the surface behaviors of H species including adsorption and spillover,[13,14] the Rh_7Pd_1 structure could induce simultaneous adsorption of H* on isolated Pd and surrounding Rh. Combined with the KIE results, the Rh_7Pd_1 structure may be beneficial to the H* spillover from Pd to surrounding Rh.

Finally, the potential of employing $Au@Rh_{7/8}Pd_{1/8}$ NWs and $Au@Ag@Rh_{7/8}Pd_{1/8}$ as practical catalysts was tested after immobilization onto SiO_2 (Fig. S17, ESI†). With a high substrate/Rh rate of 1000, ~99% of phenols could be reduced in 2 hours and the selectivity over cyclohexanone was still >80% (Table S2, ESI,† entries 1 and 5). Furthermore, although the activity is slightly lowered for the methyl-derivatives, high conversion (>90%) was achieved with the elongation of the reaction time (Table S2, ESI,† entries 2–4 and 6–8). Even for a long reaction time of 5 h, the high selectivity over cyclohexanones of 86.9 and 84.1%, respectively, again suggests that cyclohexanones are less likely to be overhydrogenated. Of note, for all the studied substrates, Au@Ag@RhPd showed higher conversion but comparable selectivity.[15] We also studied the catalysis performance of Au@RhPd and Au@Ag@RhPd for up to five successive runs, and the conversions were reduced from >98% to ~90% (Fig. S18, ESI†). The ICP-MS analysis revealed that the amount of Au was lowered by about 5%, while the Rh/Au ratio was also decreased by 1%. Therefore, we speculate that the peeling of NWs from the support is responsible for the decreased conversion.

In summary, we synthesized Au@Rh and Au@RhPd NWs as highly active catalysts for the selective hydrogenation of phenol. The underlying Au core modulated the electronic state of Rh atoms, which enhanced the adsorption of phenol, while lowering the adsorption energy for cyclohexanone and thereby increasing the activity toward the desired product cyclohexanone. The presence of isolated Pd sites would further increase the activity of Rh by providing reactive H*. This study reveals the methodology of finely regulating the atomic structure of reactive sites for superior catalysis performance. Additionally, this work shows the important role of reactive H* in the reduction reactions.

The authors are grateful for financial support from the National Natural Science Foundation of China (no. 21822608 and 21777177), Research Center for Eco-Environmental Science (RCEES-TDZ-2021-7) and the Youth Innovation Promotion Association of CAS (Y20211019).

Conflicts of interest

There are no conflicts to declare.

Notes and references

1 Q. Q. Guan, C. W. Zhu, Y. Lin, E. I. Vovk, X. H. Zhou, Y. Yang, H. C. Yu, L. N. Cao, H. W. Wang, X. H. Zhang, X. Y. Liu, M. K. Zhang, S. Q. Wei, W. X. Li and J. L. Lu, *Nat. Catal.*, 2021, **4**, 840–849.
2 H. Duan, D. Wang, Y. Kou and Y. Li, *Chem. Commun.*, 2013, **49**, 303–305.
3 H. W. Zhang, A. Han, K. Okumura, L. X. Zhong, S. Z. Li, S. Jaenicke and G. K. Chuah, *J. Catal.*, 2018, **364**, 354–365.
4 J. Zhang, Z. X. Low, Y. Shao, H. Jiang and R. Chen, *Chem. Commun.*, 2022, **58**, 1422–1425.
5 S. Wang, L. Yang, T. Zhu, N. Jiang, F. Li, H. Wang, C. Zhang and H. Song, *React. Chem. Eng.*, 2022, **7**, 170–180.
6 Y. Y. Zheng, P. S. He, Y. X. Fang, X. Yang and H. G. Liang, *RSC Adv.*, 2017, **7**, 31582–31587.
7 R. Liu, L. Q. Zhang, C. Yu, M. T. Sun, J. F. Liu and G. B. Jiang, *Adv. Mater.*, 2017, **29**, 1604571.
8 G. Chen, C. Xu, X. Huang, J. Ye, L. Gu, G. Li, Z. Tang, B. Wu, H. Yang, Z. Zhao, Z. Zhou, G. Fu and N. Zheng, *Nat. Mater.*, 2016, **15**, 564–569.
9 L. Jiang, K. Liu, S. F. Hung, L. Zhou, R. Qin, Q. Zhang, P. Liu, L. Gu, H. M. Chen, G. Fu and N. Zheng, *Nat. Nanotechnol.*, 2020, **15**, 848–853.
10 P. Liu, Y. Zhao, R. Qin, S. Mo, G. Chen, L. Gu, D. M. Chevrier, P. Zhang, Q. Guo, D. Zang, B. Wu, G. Fu and N. Zheng, *Science*, 2016, **352**, 797–801.
11 S. Schomaker and R. Holze, *Z. Phys. Chem.*, 1994, **185**, 17–32.
12 M. Dendisová-Vyškovská, A. Kokaislová, M. Ončák and P. Matějka, *J. Mol. Struct.*, 2013, **1038**, 19–28.
13 G. Feng, M. V. Ganduglia-Pirovano, C.-F. Huo and J. Sauer, *J. Phys. Chem. C*, 2018, **122**, 18445–18455.
14 L. Shi, S. Meng, S. Jungsuttiwong, S. Namuangruk, Z. H. Lu, L. Li, R. B. Zhang, G. Feng, S. J. Qing, Z. X. Gao and X. H. Yu, *Appl. Surf. Sci.*, 2020, **507**, 145162–145162.
15 M. Wollenburg, A. Heusler, K. Bergander and F. Glorius, *ACS Catal.*, 2020, **10**, 11365–11370.

